ABSTRACT

Paleoclimate and Paleoenvironment Reconstruction of Early Miocene Tinderet Sites in Western Kenya, and its Implications for Hominoid Evolution

Kennedy O. Oginga, M.S.

Advisor: Dan J. Peppe, Ph.D.

The early Miocene Tinderet sites in western Kenya preserve some the earliest occurrences of large bodied hominoids such as *Proconsul*. The sites preserve different catarrhine fossil assemblages, with some species found in all sites while others found in one site. To better assess this variation, a detailed paleoenvironmental and paleoclimatic reconstruction was done for Tinderet sites in Koru 16, Koru 21 and Kapurtay New.

The stratigraphy demonstrates that these sites sample a non-steady landscape that experienced periodic sediment input from volcanic eruptions. The lithology is comprised of interbedded ash and weakly developed paleosols that possess somewhat similar micro- and macromorphology. Paleoenvironmental reconstructions using stable carbon isotope from paleosol organic matter indicate the presence of C_3 vegetation with a likely contribution from C_4 biomass which was used in conjunction with the presence of microcharcoal from Koru and Kapurtay New to infer an environment with open patches or canopy breaks. Forest structure reconstruction in Koru 16 suggests a tropical seasonal forest with young and mature trees. Paleoclimate reconstructions using geochemical

proxies predict mean annual precipitation of >1000 mm/yr. which indicates humid conditions. Taken together, the results suggest a seasonally dry climate, and that differences in the hominoid assemblages between the sites may not be related to differences in environment or vegetation structure since this appears to be a constant factor across the localities.

Paleoclimate and Paleoenvironment Reconstruction of Early Miocene Tinderet Sites in Western Kenya, and its Implications for Hominoid Evolution.

by

Kennedy O. Oginga, B.S

A Thesis

Approved by the Department of Geoscience

Stacy C. Atchley, Ph.D., Chairperson

Submitted to the Graduate Faculty of
Baylor University in Partial Fulfillment of the
Requirements for the Degree
of
Master of Science

Approved by the Thesis Committee

Dan J. Peppe, Ph.D., Chairperson

Steven G. Driese, Ph.D.

Katie M. Binetti, Ph.D.

Stephen I. Dworkin, Ph.D.

Accepted by the Graduate School

August 2018

J. Larry Lyon, Ph.D., Dean

Page bearing signatures is kept on file in the Graduate School.

TABLE OF CONTENTS

LIST OF FIGURES

LIST OF TABLES

ACKNOWLEDGMENTS

Many thanks to my advisor Dr. Dan Peppe for giving me this opportunity of establishing my new profession as geologist. It has been a challenging and rewarding journey and I'm grateful for the advice and support I received in my studies and research. I would also like to acknowledge the support of my committee members, Dr. Steven Driese, Dr. Katie Binetti and Dr. Stephen Dworkin for their reviews and professional input to make this research a success.

A big thank you to Dr. James Lutz from Utah State University, Dr. Frederick Manthi from National Museum of Kenya, Dr. William Lukens from Baylor University and Dr. Lauren Michel from Tennessee Tech University for their academic, logistic and field support to make this research a success.

I appreciate and say a big thank you to the crew from National Museum of Kenya and local community from Koru and Kapurtay for the field support. To the National Science Foundation, Leaky Foundation, Turkana Basin Institute and Baylor University, thank you for the funding of this research.

Most importantly, to my family in Kenya, Baylor University Geoscience faculty, staff and graduate students, I humbly say thank you for the love, support and encouragement I received in the past two years.

CHAPTER ONE

Introduction

Catarrhines (cercopithecoids and hominoids) evolved as they migrated in and out of Africa during the early Miocene at a time of global climatic changes and ongoing tectonic processes that formed the East African Rift (Stewart and Disotell, 1998; Cote, 2004; Andrews and Kelley, 2007; Casanovas-Vilar et al., 2011). During this time of migration, the catarrhines occupied a large diversity of habitats and exploited many niches, some quite different from those of modern apes and monkeys (Evans et al., 1981; Jablonski, 2005; Elton, 2007; Leakey et al., 2011).

Several major early Miocene sites in East Africa such as Koru, Songhor, Kapurtay, Rusinga Island, Napak, and Moroto are known for their abundance of fossil catarrhines. The sites are considered to be roughly contemporaneous in age, between 17-20 Ma (Fig. 1; Peppe et al., 2015). Of these major fossil sites, Koru, Songhor, and Kapurtay are geographically close to each other (separated by a maximum distance of <20 km) and surround the now extinct Tinderet Volcano (Fig. 2).

Despite their close temporal and spatial proximity, the catarrhine species found at these three sites – Koru, Songhor and Kapurtay – are variable, with some species found at all sites and others restricted to only one site.

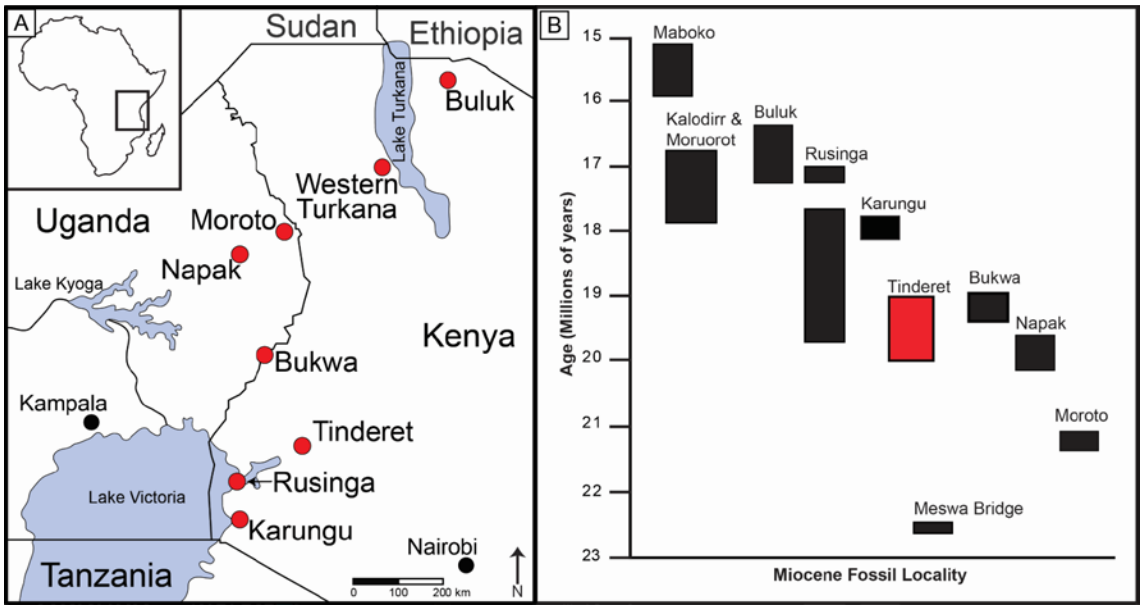

Figure 1. Major early Miocene sites in East Africa. (A) Geographic location of each site in East Africa. (B) Age estimates for the localities as reported in Peppe et al. (2015). Tinderet sites include Kapurtay, Songhor and Koru.

What drove the variation in catarrhine anatomy and paleocommunity composition between the Tinderet sites? Harrison (1982) and Pickford and Andrews (1981), suggested that the variation might be ascribed to habitat difference. However, Cote (2008) noted that paleoenvironmental reconstructions based on the faunal assemblages at the sites suggest that their habitats were essentially indistinguishable. Alternatively, the sites may not be contemporaneous and may sample different intervals of time. In this case, the faunal differences might reflect the evolution of catarrhine communities through time.

The fossil localities at Koru and Kapurtay are a key source for paleobiological information as they documents some of the earliest occurrences of large bodied hominoids such as *Proconsul major* and *P. africanus*, and other stem catarrhines (Hopwood, 1933; Martin, 1981). However, the paleoenvironment(s) of the sites are poorly understood making it difficult to assess the habitats they represent, which makes it

impossible to fully assess the driver behind the variation in catarrhine assemblages between sites.

Presented herein is an answer to the fundamental question to be addresses in this research, and that is; are the observed differences in catarrhine distribution across the Tinderet fossil sites attributable to variation in paleoenvironment between the sites? I reexamine the hypothesis that, the paleoenvironment at fossil localities in the Tinderet area forms a contemporaneous, relatively continuous, homogenous forested habitat, through a high-resolution study of interval paleosols at Koru and Kapurtay and a reconstruction of a remnant forest at Koru 16.

In this study, paleosol morphology, micromorphology, stable isotope, bulk elemental composition and mineralogy of sediments from the three sites (Koru 16, 21 and Kapurtay New site) coupled with spatial distribution of tree stump casts, were examined to present a high-resolution picture of paleoenvironment and paleoclimate.

Background and Geological Setting

The extinct early Miocene Tinderet volcano occurs in western Kenya (Muhoroni division, Kisumu County). Tinderet is surrounded by early Miocene fossil localities that occur in 6 major areas: Koru, Songhor, Kapurtay, Legetet Hill, Chamtwara, and Mtetei Valley (Fig. 2). This study will focus on reconstructing the paleoenvironment and paleoclimate of fossil localities at Koru, and Kapurtay (Fig. 2) using stratigraphic and paleopedologic methods.

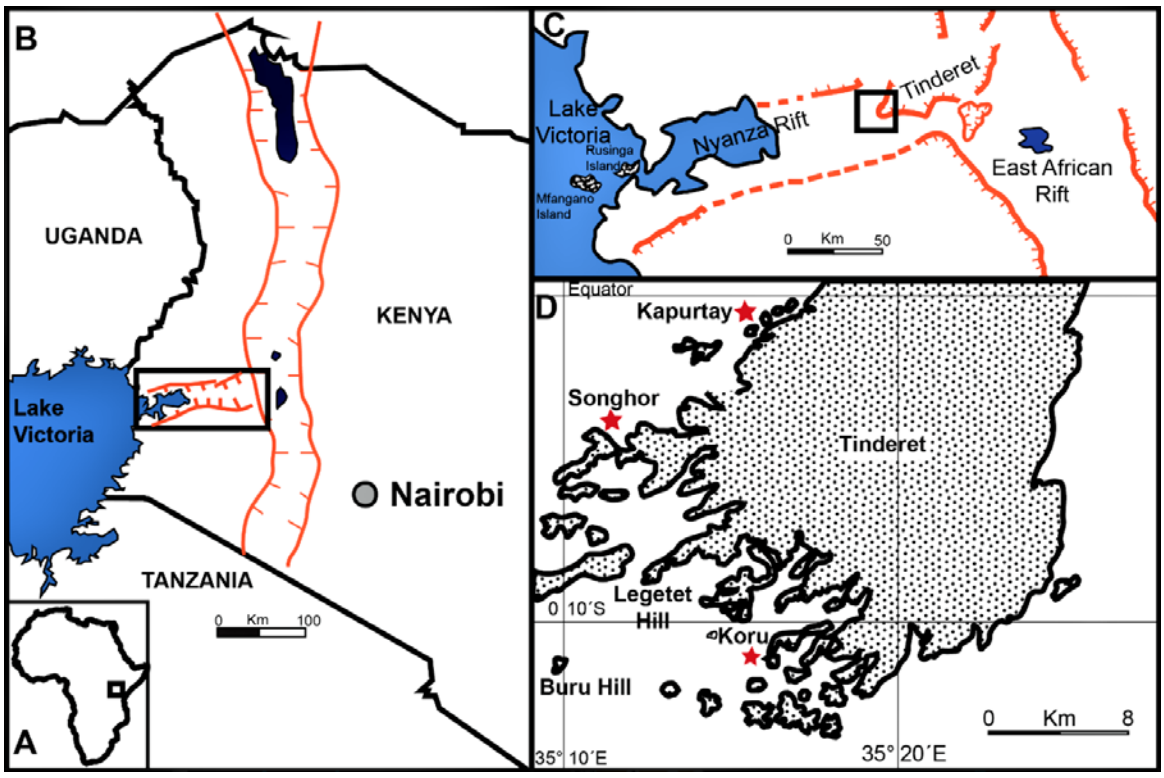

Figure 2. Locations of areas of study (A) on the African continent, and (B) within western Kenya. (C) The location of Tinderet at the Intersection of Nyanza Rift and Eastern Rift Valley. The red lines indicate fault boundary. (D) Location of the Tinderet sites around Tinderet volcano. Map modified after (Deans and Roberts, 1984). Key sites are Koru and Kapurtay indicated by the red stars.

Zaitsev et al. (2013) described the Tinderet volcano as a natrocarbonatite with similarities to the modern Oldoinyo Lengai and Kerimasi volcanoes in East Africa in terms of mineralogy, petrology and stable isotope composition. The modern Tinderet peak is located at ~15 km east of the Early Miocene fossil localities and the oldest parts of the cones are made of the same conglomerates and tuffs deposited at Koru and Songhor sites (Deans and Roberts, 1984). The deposits in the Tinderet area were originally described as lacustrine limestones by Kent (1944) and Shackleton (1951). Later Le Bas and Dixon (1965) argued that these deposits were carbonatite. Pickford (1984) later argued that although carbonatites are common in the Tinderet area, the fossiliferous

deposits are volcaniclastic and volcanogenic with very little fluvial accumulation. Preliminary research at localities in Songhor and Koru suggests that although volcanoclastic and volcanogenic deposits are most common, fluvial deposits and paleosols are locally common (Oginga et al., 2017; Peppe et al., 2015). The deposition of alkali-rich carbonatite ash is considered to be a major factor in the abundant fossil preservation at the Tinderet fossil localities (Pickford, 1986b).

The extensive faulting since the deposition of the Tinderet fossil localities, is associated with the tectonic processes that formed Nyanza and East African Rift (Fig. 2), and this in combination with a highly vegetated nature of the region today has made it difficult to reconstruct the topography at the time of deposition.

Previous research focused on reconstructing the paleoenvironment of the Tinderet sites used faunal-based paleoecological methods (e.g., Evans et al., 1981; Cote, 2008). These studies suggested that the Tinderet sites sampled a forested environment, although no climate estimates have been made. Additional research using a variety of methods is necessary to more clearly understand the paleoenvironment of the Tinderet sites.

CHAPTER TWO

Methods

Field Methods

During the summer of 2015 field season with the Research on East African Catarrhine and Hominoid Evolution (REACHE) project group, a preliminary description of Koru 16 outcrop was done. The stratigraphic succession of the early Miocene strata was measured using standard field methods and described in detail by defining 12 distinct lithostratigraphic units, starting at the base of the section. In the summer of 2017, a detailed description of paleosols and stratigraphic units of other sites – Koru 16B, Koru 21 and Kapurtay New - was done using methods outlined for paleosols adapted from modern soil description techniques (Soil Survey Staff, 2010; Schoeneberger, 2012).

Samples were collected for a series of analyses including grain size, bulk geochemistry, clay mineralogy, micromorphology and stable isotope geochemistry. Additional samples of stump casts were taken for bulk geochemistry and micromorphological analysis. Paleosol field descriptions are provided in Appendix. Tree stump casts, fossilized branches and some root casts located within the forest paleosol interval at Koru 16 site A and B were mapped across the landscape using a grid format method where the diameter and distance between the tree stump casts were measured.

Laboratory Methods

Paleosols were sampled by horizon for oriented thin sections, which were subsequently prepared by a commercial laboratory (Spectrum Petrographics. Inc.) as 5 ×

7 cm thin-sections. The thin sections were examined at Baylor University using an Olympus BX51 Research microscope equipped with a standard plane-polarized (PPL) and cross-polarized (XPL) light, as well as with UV fluorescence (UVf). Micromorphological descriptions and interpretations followed the descriptions given by Brewer (1964) and Bullock et al. (1985).

Elemental geochemistry of bulk paleosol samples were analyzed using ICP-AES and ICP-MS for major and trace elements at ALS Global (alsglobal.com). Clay minerals from bulk samples of paleosols from the three sites were separated by dispersal and centrifugation following methods of Poppe et al. (2001), and the clay separates were then treated and oriented using the Millipore filter transfer method (Moore and Reynolds, 1997). All the samples were then scanned over a range of 2–30° 2Θ with a step size of 0.02° 2Θ and dwell time of 1 s, using a Siemens D5000 Θ-2Θ X-ray diffractometer with Cu–Kα radiation operating at 40 Kv and 30 mA.

Samples for total organic carbon and $\delta^{13}C$ stable isotope analysis were first homogenized using shatterbox. Approximately 1 g of samples were then loaded on glass centrifuge tubes and treated with 10% HCl until visible reaction stopped. Samples were then rinsed with distilled water and centrifuged at 1500 rpm. The treatment with 10% HCl and rising process was repeated three times before samples were submitted for analysis. Samples were then loaded in a Costech EA coupled to a Delta V® mass spectrometer via a Thermo Scientific Conflo IV interface at Baylor University. Replicate analyses for standards were run with a standard error of <0.04‰. All sample values were normalized to Vienna Pee Dee Belemnite (VPDB) using repeat analyses of two in-house standards and are reported in standard per mil notation (‰) relative to VPDB, where;

$$\delta^{13}C = \frac{R^{13}_{Sample} - R^{13}_{Std}}{R^{13}_{Std}} \times 1000$$ and R = $^{13}C/^{12}C$.

Paleosol Climofunctions

Bulk geochemistry of paleosol B horizons was used to estimate mean annual precipitation (MAP) and mean annual temperature (MAT) using climofunctions described by Sheldon et al. (2002), and Nordt and Driese (2010). MAP was estimated using the chemical Index of alteration minus Potassium (CIA-K) proxy of Sheldon et al. (2002), defined as $100\times[(Al_2O_3)/(Al_2O_3+Na_2O+CaO)]$, where the oxides are normalized to their respective molecular weights. The CIA-K pedotransfer function is measure of feldspar hydrolysis and leaching of its cations, and designed to be used in well-drained B horizons in which there has been sufficient time for soil formation to equilibrate with climate conditions. Another proxy used in this research is CALMAG (Nordt and Driese, 2010) designed for application in well-drained B horizons of paleo-vertisols, and is defined as $100\times[(Al_2O_3)/Al_2O_3+CaO+MgO)]$, and all oxides normalized to their respective molecular weights. This proxy is mainly a measure of loss of exchangeable base cations in Vertisols associated with increased rainfall.

The salinization proxy of Sheldon et al. (2002), which is defined as $[(K_2O+Na_2O)/(Al_2O_3)]$ – all oxides normalized to their respective molecular weights – was used to estimate MAT. This proxy is used for B horizons of well-drained paleosols over the temperature range of 8°C – 22°C. NaK is based on the thermodynamic dissolution of silicates, primarily feldspar, occurring more rapidly at higher temperatures.

The paleosol-paleoclimate model ($PPM_{1.0}$) by Stinchcomb et al. (2016) was also used to predict MAP and MAT. $PPM_{1.0}$ was developed using data from 648 modern soil

B horizons. The model uses eleven oxides (Fe_2O_3, Al_2O_3, SiO_2, TiO_2, ZrO_2, CaO, MgO, K_2O, Na_2O, MnO and P_2O_5) as input variables reduced to four regressors using partial least squares regression. The regressors are then modeled using thin-plate spline that predicts MAP and MAT. The calculations were done using SAS statistical software (SAS Institute, Inc., v. 9.2).

Stable Isotope Analysis of Paleosol Organic Matter

The framework for vegetation reconstruction using stable isotopes is based on photosynthetic pathway of plants that differentially fractionate atmospheric CO_2, resulting in soil organic matter with different $\delta^{13}C$ signatures. The Calvin cycle, a C_3 pathway, is used by most trees and shrubs and produce soil organic matter (SOM) with a $\delta^{13}C$ between –20 to –33‰ with a mean of –26.7‰ (O'Leary, 1981, 1988; Cerling et al., 1997). In water-stressed environments, the $\delta^{13}C$ signature of C_3 plants ranges from –24 to –25‰ (Ehleringer and Cooper, 1988). Hatch-Slack, a C_4 pathway, is used by modern tropical and warm-season grasses and sedges which produce SOM with a $\delta^{13}C$ signature between –9 to –16‰ with a mean value of –12.5‰ (O'Leary, 1981, 1988; Cerling et al., 1997). C_3 plants are the most dominant type of vegetation in forest environments and therefore their $\delta^{13}C$ signatures should resemble that of a dense forest with most negative values as expected in tropical forests which have an isotopic signature more negative than –30‰ (Ehleringer, 1978; Ehleringer and Cooper, 1988; Ehleringer and Monson, 1993; Cerling et al., 1997; Kohn, 2010).

The $\delta^{13}C$ composition for C_3 and C_4 plants were modeled using fractionation factors for each photosynthetic pathway that were corrected for atmospheric CO_2 composition of –6.0 ± 0.2‰ from benthic foraminifera for early Miocene (18.45 to 20.15

Ma)(Tipple et al., 2010). Fractionation factors used were –19.6‰ for C_3 plants, –16.7‰ for water stressed C_3 plants and –4.7‰ for C_4 plants (Passey et al., 2002).

CHAPTER THREE

Results

Stratigraphy and Sedimentology

The lithology of Koru 16, Koru 21 and Kapurtay New describes lithofacies characterized interbedded ash and weakly developed paleosols. Koru 21 stratigraphy comprises compound paleosols bounded by lithified carbonatite ash deposits while Koru 16 and Kapurtay New stratigraphy comprises interbedded ash and weakly developed paleosols.

Koru 16A and 16B Sites.

The stratigraphic section at Koru 16 is 7 m thick with 12 distinct lithologic units in site A, and 2 m thick with 2 distinct lithologic units in site B which can be correlated to site A (Fig. 4). The basal unit in Site A is well developed paleo-vertisol that is described below. The paleosol is abruptly overlain by a series of weathered and unweathered ash deposits that vary in lithology. The ash deposits are then abruptly overlain by a series of paleo-Inceptisols (units 6, 7, and 8). These paleosols are highly calcareous and abundant in unweathered volcanic minerals.

Three stratigraphic units (paleo-Vertisols unit 1 and 8, and unit 7) that represent the key depositional environment were analyzed in detail. The paleo-Vertisol comprising unit 1 in the measured section is at least 37cm thick with color ranging from dark red (10R 4/6) to dark reddish brown (2.5YR 3/4). This paleosol is non-calcareous and has a high clay content (>65%), well defined pedogenic slickenside surfaces, medium wedge-

shaped peds parting to angular blocky peds, fine root traces, and minor-chroma color mottling (Fig. 3A; Appendix). Three horizons were identified and described, a Bt2, Btss2 and Bss2.

Unit 7, a paleo-Inceptisol, is characterized by laminations that increase in thickness upwards and accretionary lapillis that are highly weathered into clay at the base and relatively unweathered at the top of the unit. These observations were also made on the basal unit in site B (Fig. 4). Poorly preserved fossil leaves are also preserved on Unit 11. Tree stump casts were identified in both sites A and B (Fig. 3D). Also present were calcite-cemented roots, tree branches (Fig. 3E) and poorly preserved fossil leaves. A total of 7 tree stump casts were identified in site A and 5 in site B. Horizonation is Bw for both paleosols in Site A and B.

Overlying the paleo-Inceptisols is another weakly developed vertisol (Unit 8) with two distinct horizons, Bt1 and Btss1. This paleosol is less calcareous judging from the weak reaction to acid. Faint slickensides, moderately developed ped structure, drab haloed root traces and illuviated clay on slicken side surfaces characterize the horizons (Fig. 3 C and D). Root traces are very fine and no pedogenic carbonates were identified.

At the top of the section (Unit 10) is another weakly developed paleosol that shares characteristics with the underlying Inceptisols in Unit 6 and 7. The overlying deposit (Unit 11) is another weathered ash deposit with poorly preserved fossil leaves.

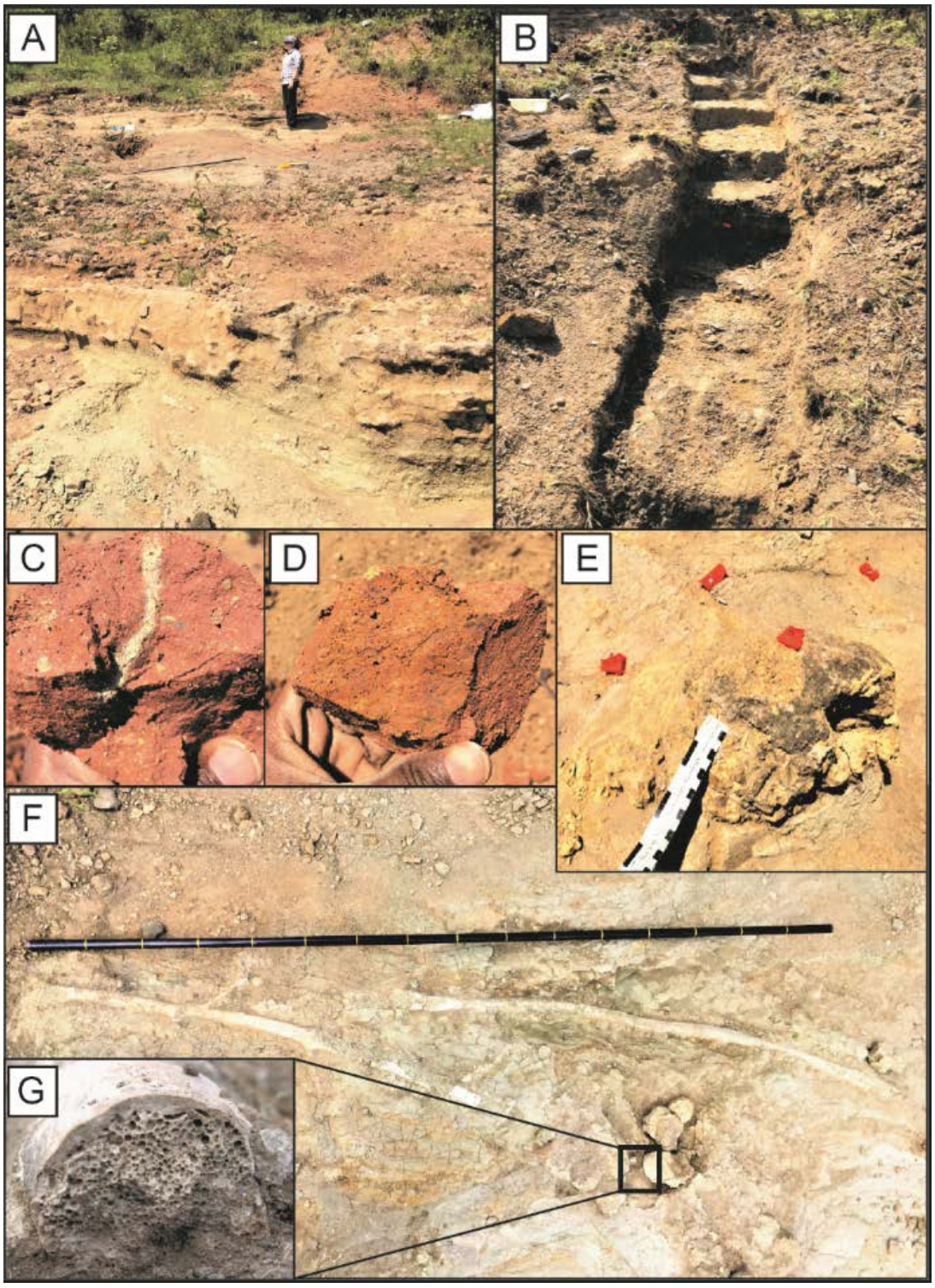

Figure 3. Field photographs of Koru 16 site. (A) Koru 16 profile A and (B) Koru 16 profile B. (C) Drab haloed root trace from upper paleo-vertisol. (D) Slickenside surface with illuviated clay from the basal paleo-vertisol. (E) One of the tree stump cast preserved in the "forest paleosol" (unit 7). (F) Fossilized tree branch. Note the opposite branching shown by the red arrow. (G) The internal structure of the calcified tree branch.

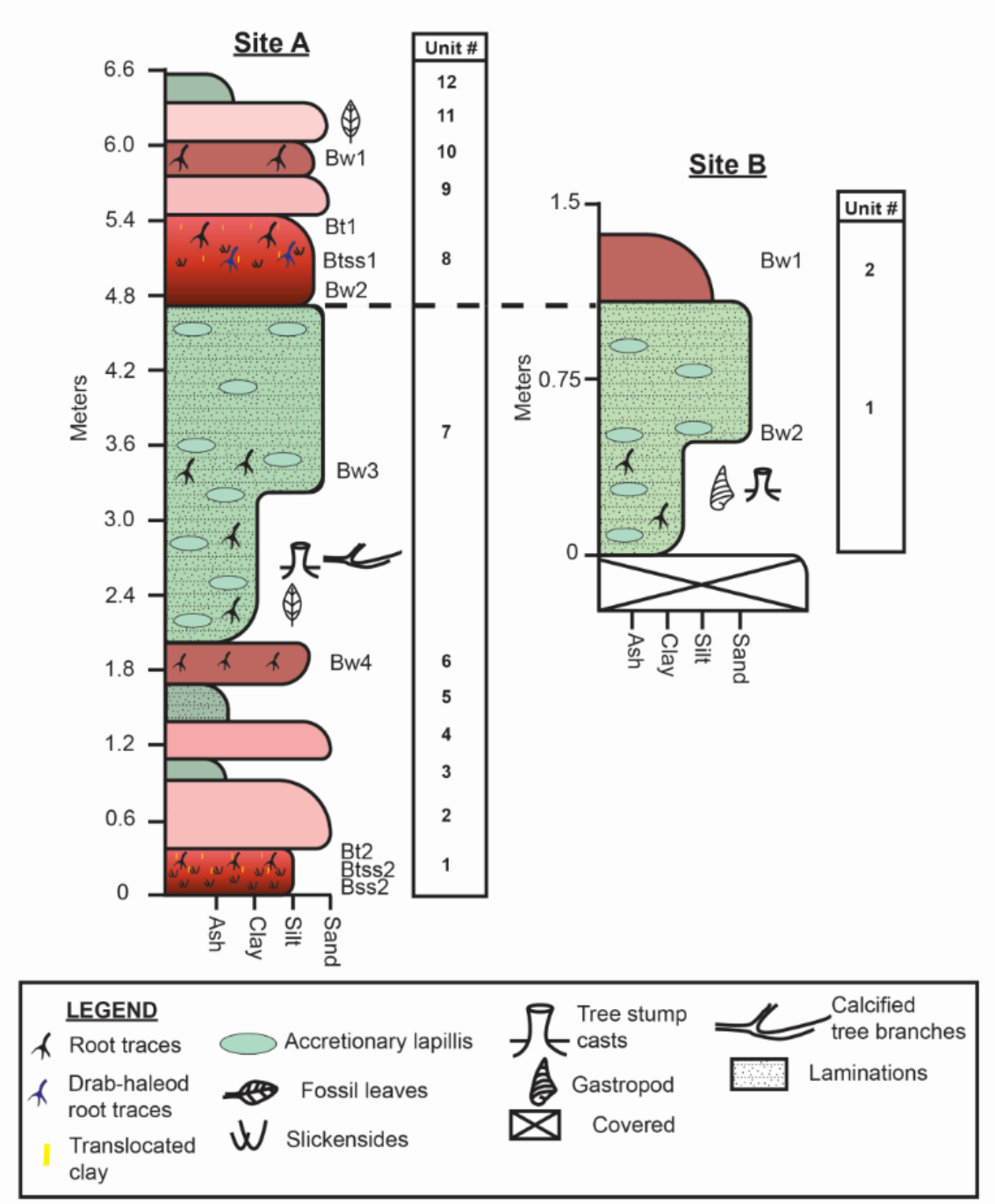

Figure 4. Stratigraphic column of the two profiles from Koru 16 site A and B. The two profiles are correlated using the laminated paleosol intervals. Horizonations of the paleosols are also indicated. See appendix for more details on the descriptions of the paleosols.

Koru 21 Site

The stratigraphic section at Koru 21 is 7 m thick with 3 distinct lithologic units (Fig. 5). The stratigraphy records a landscape that is somewhat similar to that of Koru 16. The depositional environment is also subaerial with little fluvial accumulation. The lithology basically comprises superimposed paleosols bounded by lithified carbonatite ash (Fig. 5A). The stacked paleosols are weakly developed and demonstrate similar pedogenic development to Koru 16 and Kapurtay New paleosols.

Horizonation consists of interbedded Bw and BC horizons (Fig. 7A). Overall, the paleosols have a poorly-developed ped structure with little clay accumulation and color ranging from red (2.5YR 5/6) to pale red (2.5YR 7/2). The sediments are highly calcareous and abundant in unweathered volcanic minerals such biotite. Fine root traces were observed in the Bw's horizon and gastropod shells preserved on the upper contact of the lithified carbonatite ash.

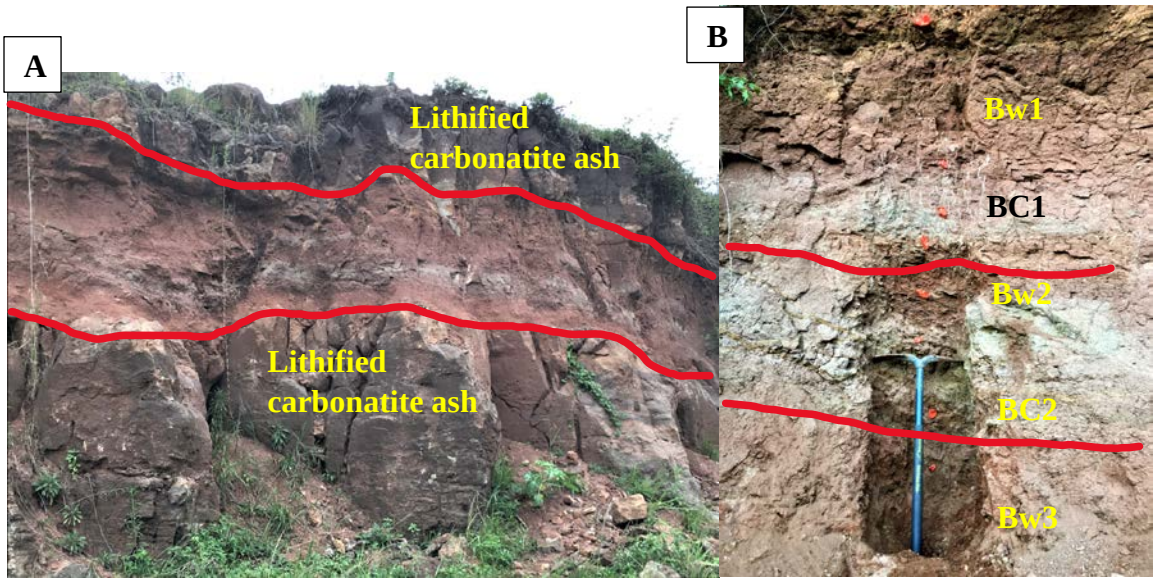

Figure 5. Field photographs of Koru 21 site. (A) The outcrop showing the paleosol bounded by two lithified carbonatite ashes. (B) Horizonation of the superimposed paleosols. Red line demarcates the contact between the paleosols.

Kapurtay New Site

Kapurtay New stratigraphic section is 22 m thick with 12 distinct lithologic units (Fig. 7B). The outcrop is poorly exposed with some parts of the section covered with modern sediments and vegetation. The lithology comprises interbedded ash and poorly developed paleosols (Fig. 7). The paleosols identified are thin and possess similar characteristics as the Koru 16 and 21 Inceptisols (see the paleosol descriptions in Appendix). These Inceptisols are highly calcareous, have a weakly developed ped structure, clay accumulation is minimal and there's high abundance of unweathered volcanic materials. Pedogenic Fe oxide nodules on ped faces and fine root traces can also be observed. Horizonation is Bw with color ranging from reddish-brown (2.5YR 5/4) to light reddish brown (2.5YR 6/3). At the top of the outcrop is a lahar flow or an agglomerate. Bone fragments and gastropod shells were found preserved in situ on Unit 4.

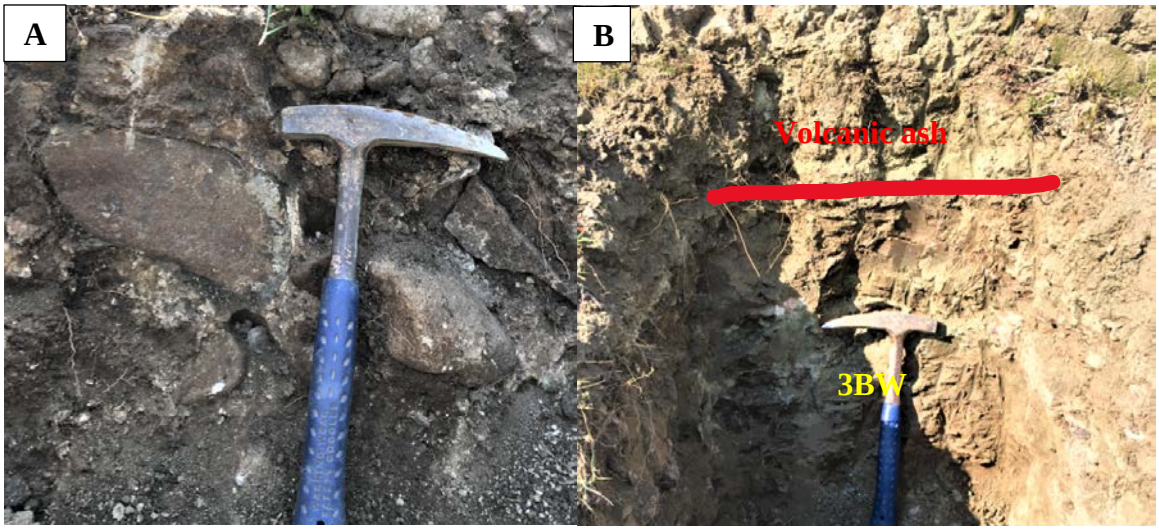

Figure 6. Field photographs of Kapurtay New. (A) Conglomerate deposit overlying the basal unit. (B) An Inceptisol bounded by a volcanic ash deposit. Red line marks the boundary between the two layers.

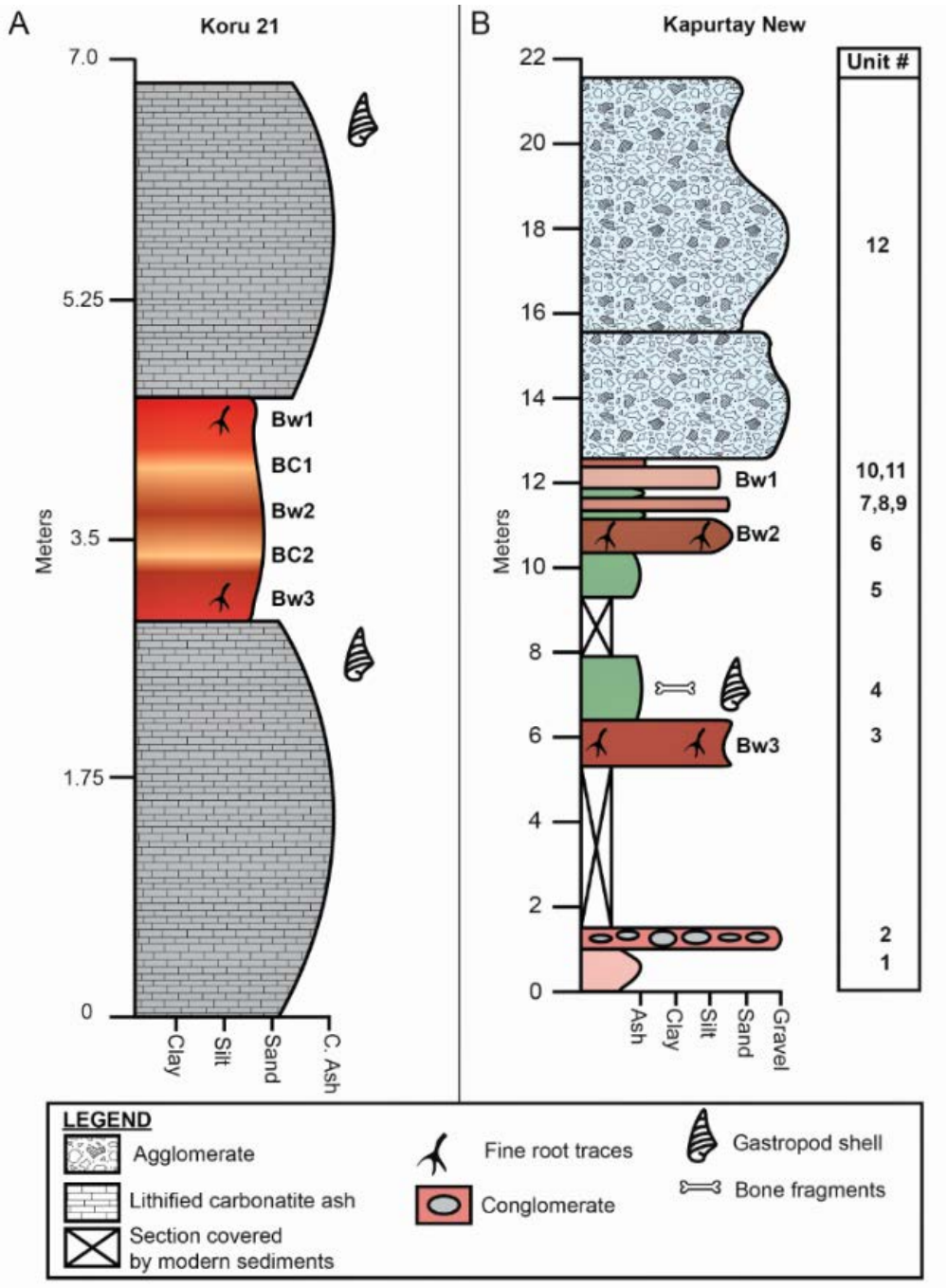

Figure 7. Lithostratigraphic section at Koru 21 and Kapurtay sites. **(A)** Koru 21 profile showing the superimposed paleosols bounded by lithified carbonatite ash. **(B)** Kapurtay New profile showing the interbedded ash and paleosol deposit with an agglomerate and a conglomerate deposited at the top and bottom respectively.

Micromorphology

Examination of thin-sections prepared from all the paleosol horizons revealed a variety of diagenetic, pedogenic and sedimentary features as well as evidence for poor weathering and leaching of volcanic minerals.

Koru 16A Profile

Six thin sections prepared from Koru 16A paleosols and tree stump casts were both studied for a pedogenic and diagenetic features. The Bt2 and Btss2 horizons from the basal paleo-Vertisol have a blocky micro-ped structure. Most grains are angular in shape and show little to no evidence of alteration (Fig. 8A, B & C). Matrix is dominated by a moderately developed b-fabric which is oriented around grains (Fig. 8A). Root traces are characterized by redox features along the walls (Fig. 8C). Pedogenic carbonate nodules were also identified from the Btss1 horizon of Unit 8 paleosol (Fig. 8B). Although both paleo-Vertisols seem to be well-drained, unweathered volcanic minerals such as feldspar and biotite are still present in all the horizons (Fig. 8A & C).

The forest paleosol differs slightly in micromorphology as compared to other paleosols. The matrix is Fe and Mn depleted and but rich in reprecipitated sparry calcite with a rhombohedral crystal shape and cleavages. Fe and Mn oxide present occurs as typic Fe/Mn oxide nodules (Fig. 8E). Most grains are angular in shape and coated with either clay or very fine sediments. The accretionary lapillis in the paleosols weather into clay (Fig. 8E) and the tree stump casts are characterized by pisoids nucleating around volcaniclastic detritus (Fig. 8F).

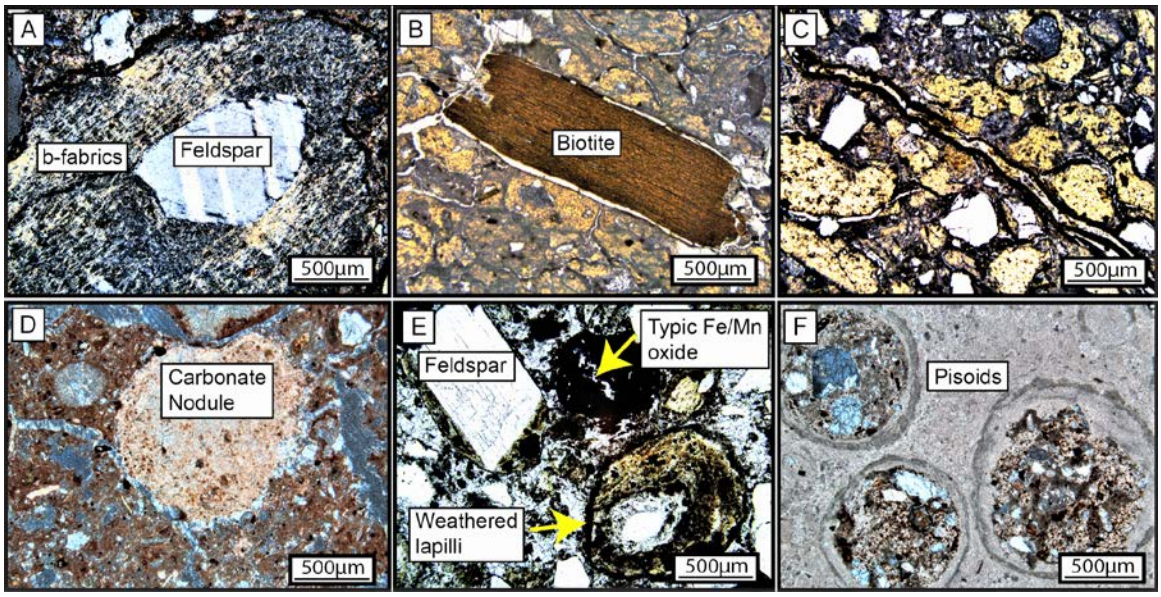

Figure 8. Photomicrographs of thin sections from the paleo-Vertisol and forest paleosol interval. K16-01-Bt2; (A) Moderately developed b-fabrics oriented around feldspar grain (XPL). (B) Blocky micro-ped structure and unweathered biotite (PPL). (C) Angular grains and root pore with FeMn lining on the walls of the root pore (PPL). (D) K16-07-Btss1; Fe rich matrix and pedogenic carbonate nodule (XPL). (E) FP-01-Bw3; Weathered lapilli, coated feldspar grain and a typic Fe and Mn oxide nodule (PPL). (F) ST-01; pisoids nucleating around volcaniclastic detritus (XPL).

Koru 21 Profile

Two thin section from Bw2 and Bw3 horizons in Koru 21 paleosol were examined. The paleosols show similar characteristics as Koru 16 paleosols with minor differences. The paleosols are also volcaniclastic-rich and most grains are angular in shape and show little to no evidence of alteration (Fig. 9B). Bw3 horizon is Fe rich in the matrix which has a weakly developed b-fabrics. Pedogenic carbonate is reprecipitated on cleavages around the surface of grains (Fig. 9A). The Bw2 horizon differs from the Bw3 horizon, in that, pore spaces and root traces are characterized by reprecipitated sparry calcite with rhombohedral crystal shapes and cleavages (Fig. 9 C & D). Grains are

angular in shape and coated with fine clay size sediments. Redox features such as typic Fe and Mn oxide nodules were also identified (Fig. 9 C & D).

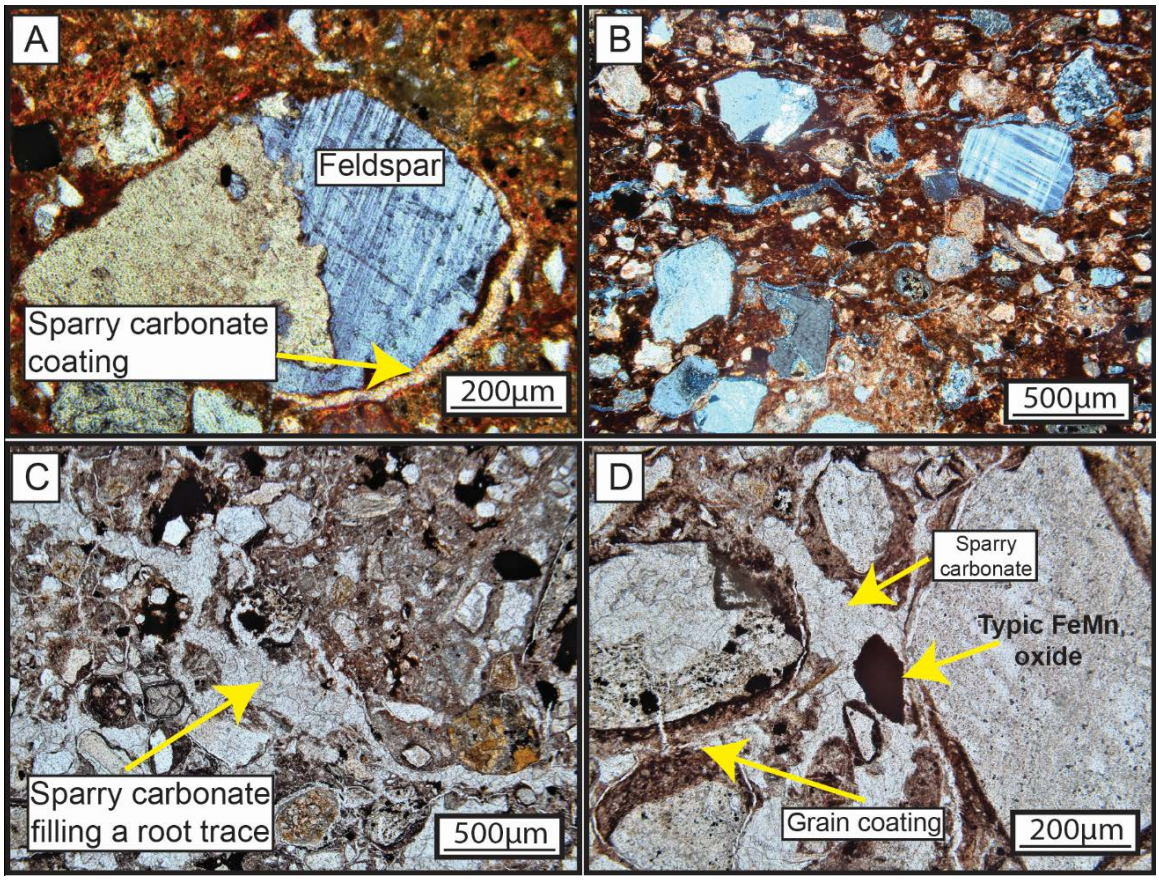

Figure 9. Photomicrographs of thin sections from Koru 21 site. (A) K21-01-Bw3; Moderately developed b-fabric and sparry carbonate precipitated on a cleavage around the surface of a felspar grain (XPL). (B) Blocky micro-ped structure and matrix that is Fe and carbonate rich. Framework grains are angular in shape and comprised of volcanic minerals (XPL). (C) K21-04-Bw2; Fe-depleted matrix and root trace filled with reprecipitated sparry carbonate; angular framework grains with Fe/Mn oxide nucleating around the surface (PPL). (D) Grains coated with fine clay size sediments; typic Fe/Mn oxide nodule and sparry calcite filling pore spaces (PPL).

Kapurtay New

Two thin section from the two paleosols were examined for the Kapurtay New site. Similarly to Koru 16 and Koru 21 paleosols, Kapurtay New paleosols are also abundant in unweathered volcanic detritus that are angular in shape and show little to no

evidence for alteration (Fig. 10 A & D). In Bw3 horizon, the matrix is characterized by a weakly developed b-fabric which appears to be oriented around some grains while others are coated with sparry carbonate which could be pedogenic (Fig. 10A & B). Unweathered volcanic minerals are abundant in both horizons. In Bw3 horizon, micro-charcoal grains were identified (Fig. 10C).

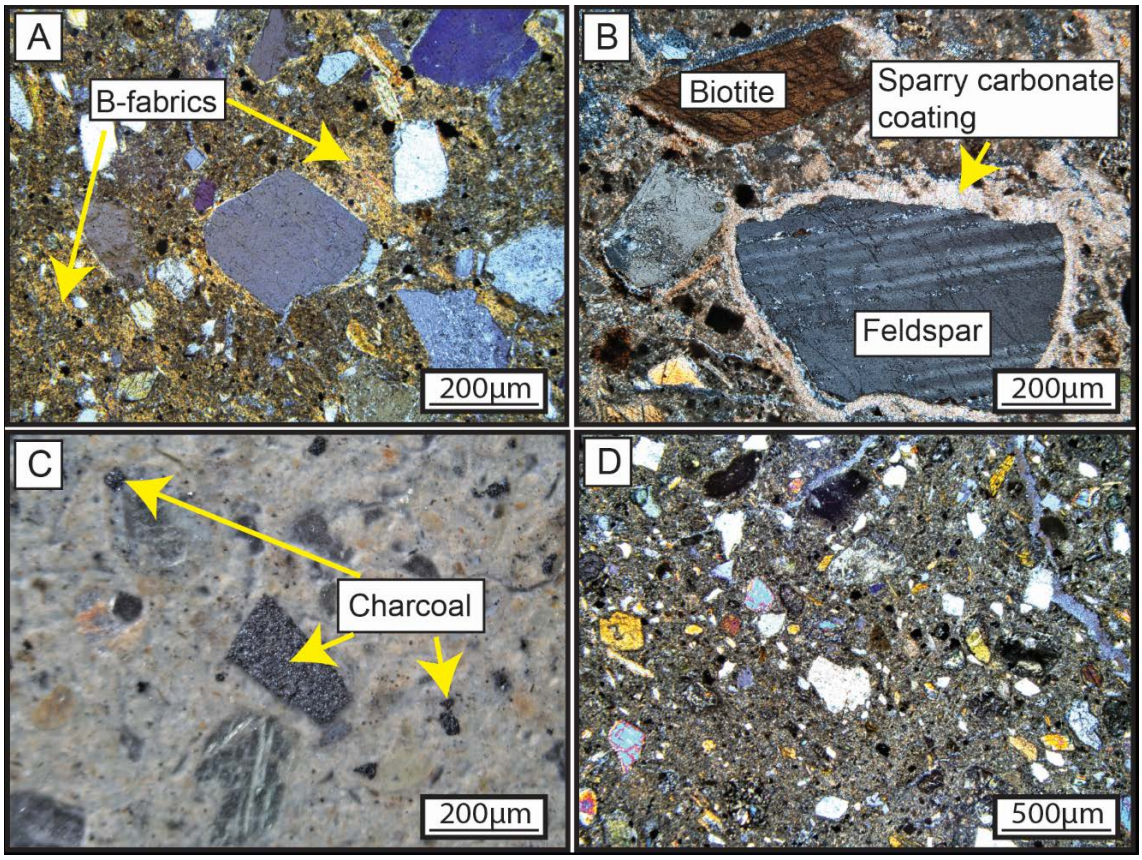

Figure 10. Photomicrographs of thin sections for Kapurtay New site. (A) KP-01-Bw3; Weakly developed b-fabrics oriented around a quartz grain (XPL). (B) Unweathered biotite and feldspar grains with sparry carbonate precipitated around the surface (XPL). (C) Micro-charcoal grains (Reflected light). (D) KP-02-Bw2; Weak b-fabrics and angular grains comprising of volcanic minerals (XPL).

Clay Mineralogy

Samples analyzed from the three sites yielded a largely similar X-ray diffraction results (Fig. 11). One clay mineral was identified with a primary peak at ~15.6 Å. The

peak shifts to ~17.1Å upon treatment with glycerol and collapses to ~9.8 Å when heated to 550°C (Fig. 11).

Based on these characteristics the clay mineral was identified to be smectite. Sample collected from Bw3 (319 cm) in Koru 21 reveal another mineral in its diffractogram (Fig. 11E) with a primary peak at ~10.1 Å, 5.03 Å and 3.35 Å which remains unchanged upon treatment. The lack of change with glycerol or heating treatments supports an interpretation of a mica mineralogy given the abundance of this mineral as observed in thin sections (Fig. 8 and 10). Peaks associated with kaolinite (7.18 Å and 5.38 Å) were not observed from the diffractogram of all the samples.

Paleoenvironment Reconstruction Using Stable Isotope

The $\delta^{13}C$ of paleosol organic matter was measured from all the B horizons of paleosols in all the three sites (raw data in Appendix table 3). The values range from –19.47 ‰ to –25.64 ‰ (Fig.12). Isotope values are broadly similar between the three sites with Koru 16, Koru 21 and Kapurtay New having mean isotopic values of –23.53‰, –22.98 ‰ and –23.64‰ respectively. All samples analyzed fall within the range of $\delta^{13}C_{3ws}$ endmember composition with exception of one Koru 21 sample from Bw3 horizon (Fig. 12).

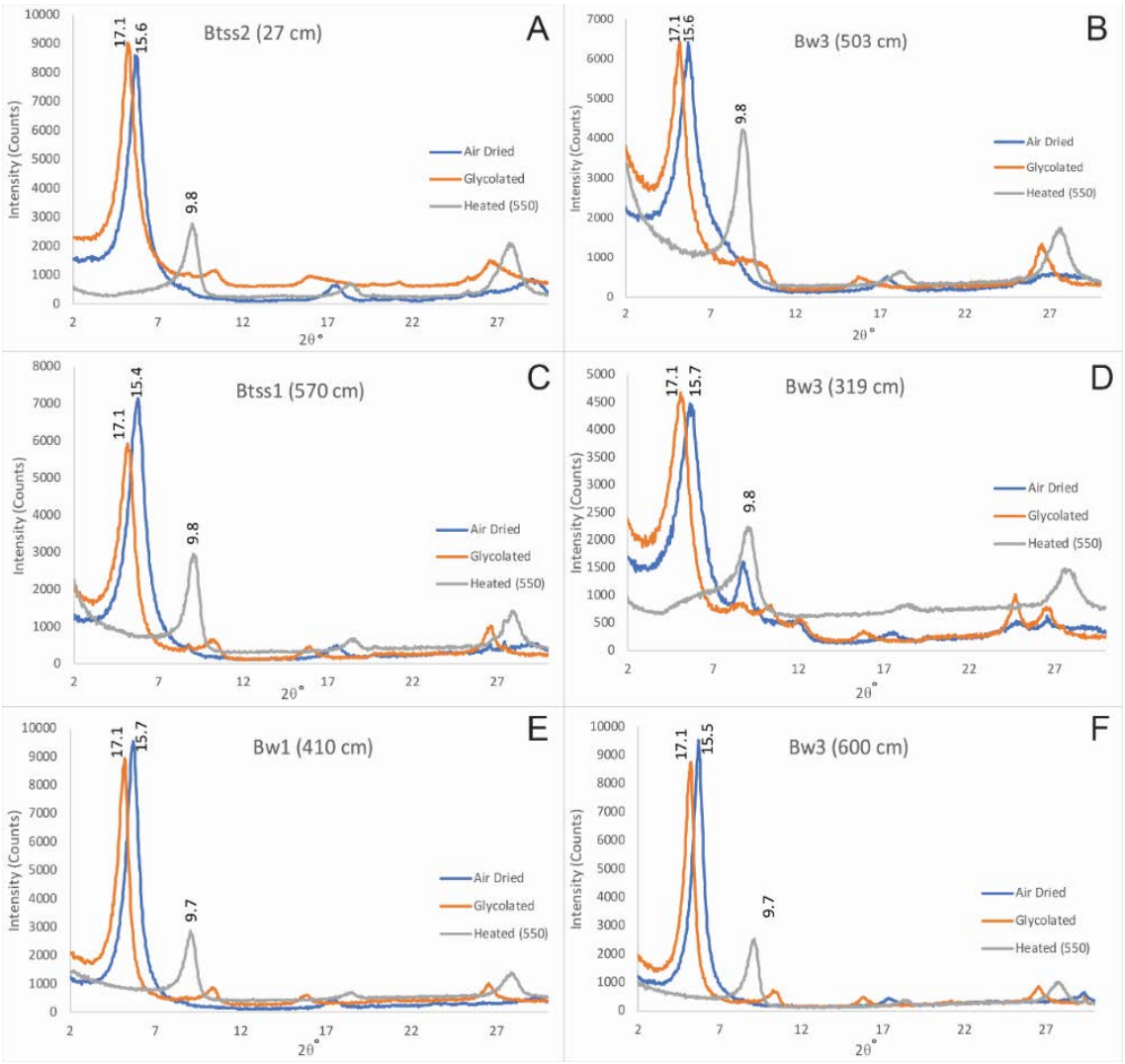

Figure 11. X-Ray diffractogram of oriented aggregates of the <2 µm fraction. Six horizons from the three sites were analyzed: From Koru 16A, (A) Btss2 from the basal paleo-Vertisol, (B) Bw3 from the Unit 7, and (C) Btss1 from the Unit 8. From Koru 21, (D) Bw3 and (E) Bw1. From Kapurtay New, (F) Bw3. The samples were subjected to three treatments: Air-dried, glycerol solvation and heating to 550°C for 1 hr. Smectite is identified by a peak at ~15 – 16 Å in the air-dried treatment, which shifts to a higher d-spacing at ~17 – 17.5 Å with glycerol solvation and collapses to ~10 Å when heat-treated at 550°C.

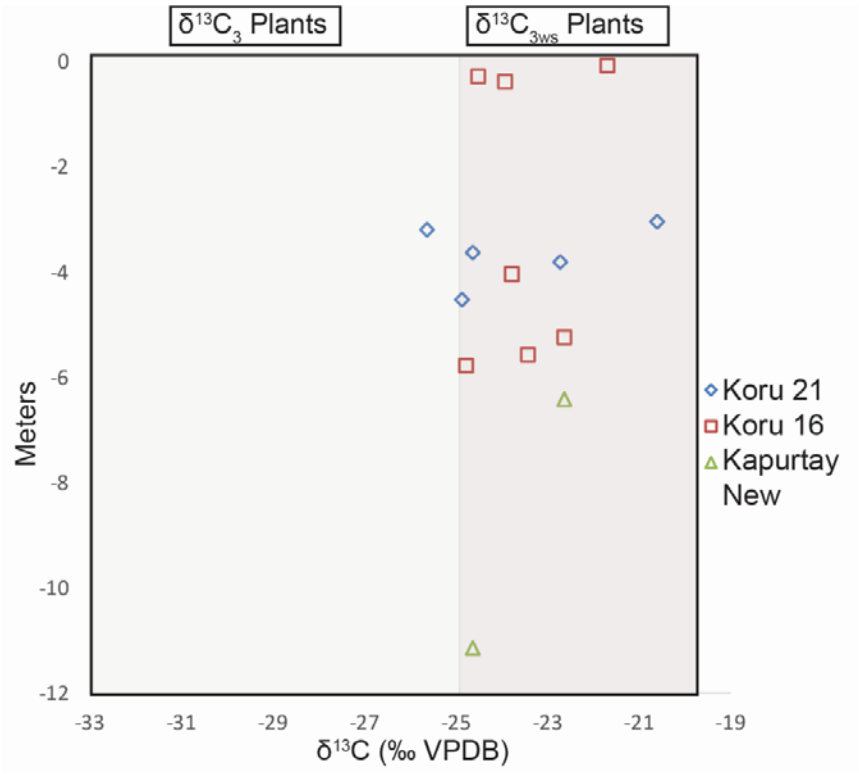

Figure 12. Stable isotope composition of SOM from the three Tinderet sites. Cross plot of $\delta^{13}C$ composition vs. depth in meters with calculated endmember composition for C_3 and water-stressed C_3 (C_{3ws}) vegetation.

Paleoclimate Reconstruction Using Paleosol Geochemistry

For paleoclimate reconstruction, weathering index proxies and a multivariate spline model were employed to estimate MAP and MAT using paleosol geochemistry. CIA-K and CALMAG for MAP yielded humid estimates ranging from 1000 to 1200 mm/yr. for the three sites. (Table 1). PPM model similarly yielded humid estimates >1000 mm/yr. More details on why the proxies underestimated MAT and MAP are in the discussion chapter below. MAT predicted by NaK, and the PPM model are within the mesic zone (10 – 15°C) for all the three sites, which is unrealistic given the equatorial positions of these sites in the Early Miocene.

Table 1. Paleoclimate proxies. PPM model done using SAS statistical software as outlined in Stinchcomb et al. (2016). Elemental oxides for CALMAG, CIA-K, and Salinization proxy expressed in mole wt. %.

Proxy	Index	Index Formula	Koru 16	Koru 21	Kapurtay New
Mean annual precipitation (mm/yr.)					
CALMAG (Nordt and Driese, 2010b)	100× $[(Al_2O_3)/(Al_2O_3+CaO+MgO)]$	$y = 22.69(x) – 435.8$	593 – 1132	468 – 980	518 – 908
Chemical Index of Alteration Minus – Potassium (CIA-K) (Sheldon et al., 2002)	100 × $[Al_2O_3/(Al_2O_3+CaO+Na_2O)]$	$y = 221.1e^{0.02(x)}$	557 – 1074	556 – 887	715 – 906
PPM (Stinchcomb et al., 2016)	NA	Thin plate spline	635 – 2035	1090 – 1968	626 – 971
Mean annual temperature (°C)					
Salinization (Sheldon et al., 2002)	$(Na_2O + K_2O) / Al_2O_3$	$y = −18.52(x)+17.298$	10 – 14	11 – 14	10 – 13
PPM (Stinchcomb et al., 2016)	NA	Thin plate spline	10 – 15.6	12 – 15	14

Forest Reconstruction

Following methods used by Michel et al. (2014), reconstruction of the forest structure using diameter and spatial distribution of stump casts (Fig. 13 A and B) shows that forest density of trees with a diameter at breast height (dbh) ≥30 cm was ≥136 trees/ha and that basal area of trees with dbh ≥30 cm was ≥13.7 m^2/ha. This places Koru 16 among less dense forests like Yasuni forest in Ecuador and Huai Kha Khaeng forest in Thailand (Table 2). This forest patch was composed of mature trees (30-45 cm dbh), but did not include trees ≥60 cm dbh as found on Rusinga Island (Michel et al., 2014) and in older tropical forests.

Table 2. Comparison of Koru 16 forest reconstruction to modern forests and early Miocene forest from Rusinga. Contemporary primate occurrence from field reports.

Forest	Sampled area (ha)	Tree basal area (m2/ha)		Tree density (trees/ha)		Primates
		≥30 cm DBH	≥60 cm DBH	≥30 cm DBH	≥60 cm DBH	
Yasuni, Ecuador	50	13.4	4.1	81	8	Yes
Huai Kha Khaeng, Thailand	50	20.7	12.1	102	13	Yes
Koru 16	0.03	13.7	-	136	-	Yes
Rusinga Island (Mean)	0.09	39.6	22.2	173	48	Yes

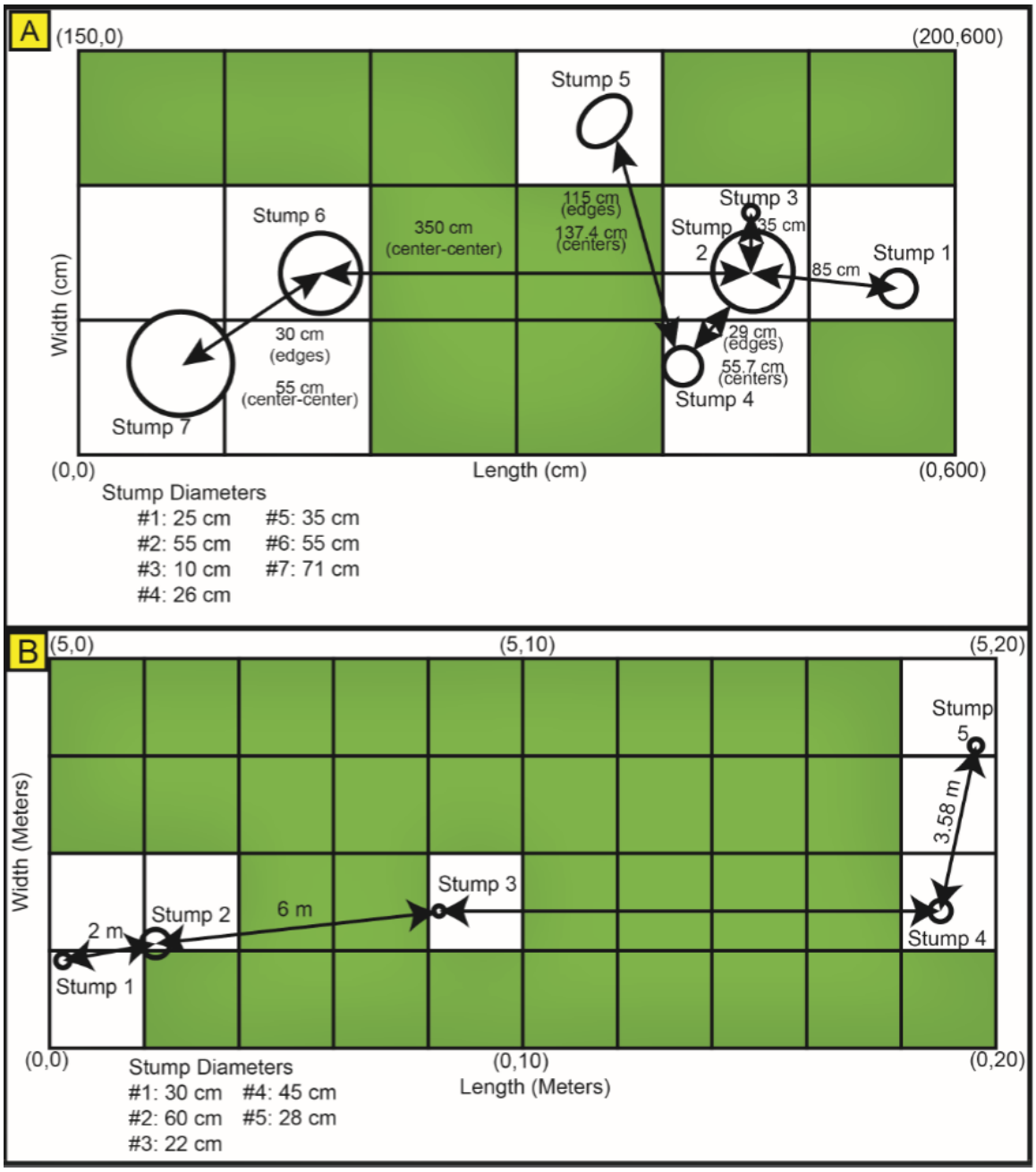

Figure 13. Spatial distribution of tree stump casts across the forest paleosol at Koru 16. (A) and (B) An illustration of the spatial distribution of the tree stump casts and the diameters of each cast for site A and B respectively. Areas shaded in green indicate absence of stump casts. The circles indicate a tree stump cast. Maps drawn to scale

CHAPTER FOUR

Discussion and Interpretation

Environment of Deposition

The lithology of Koru 16, Koru 21 and Kapurtay New sites display many similarities in terms of macro and micromorphology which provide a basis for reconstructing paleoclimate and paleoenvironment. Most sediments at all of the sites have been pedogenically and diagenetically modified with ash deposits interbedding paleosols. The depositional environment is subaerial and categorized as a non-steady aggrading landscape with minimal erosion resulting to weakly developed compound paleosols interbedded by ash deposits.

Presence of weatherable volcanic minerals such as feldspar, pyroxene and biotite, poor leaching of mobile elements and weak horizonation indicates that the paleosols had a short duration of time to develop and the rate of sedimentation outpaced pedogenesis. Kapurtay New paleosols are thin and more poorly developed which suggests that sedimentation was more rapid as compared to Koru sites.

In unit 7 interval at Koru 16, the variation in thickness on laminations of air fall tuff deposits suggests that at the inception, minor eruptions provided nutrients such as nitrates and phosphates which supported the growth of the forest, but with time the eruptions became lager – judging by the thickness of beds, which become thicker towards the upper contact of the paleosol – and likely destroyed the forest.

The presence of illuviated clay, well developed ped structure, pedogenic carbonate and slickensides in the paleo-Vertisols indicates well-drained conditions and seasonality (wet and dry conditions). Contrary, the occurrence of Fe and Mn depleted zones in Koru 16 forest paleosol and Koru 21 Bw2 horizon suggests saturated conditions brought about by periods of poor drainage or ground water movement.

The clay mineralogy of the three sites is similar with smectite being the dominant clay mineral (Fig. 11). Illite and kaolinite was notably absent from all the sites. One sample from Koru 21 collected from the Bw3 horizon has a peak at 10Å which remains unchanged upon treatments. This is characteristic of an illite or mica. Given the abundance of mica in all observed samples, it is plausible that this peak is mica rather than illite. The occurrence of smectite is attributed to precipitation from fluids containing elements from alteration of Si-, Al-, Fe- and Mg-bearing minerals such as feldspar, biotite and pyroxene (Odom, 1984). Increase in Al_2O_3 relative SiO_2 would signify pedogenic clay which was not the case. This suggests that the clay fabrics observed in thin section and slicken side surfaces are primarily diagenetic clays.

Paleoclimate Reconstruction

Bulk geochemical proxies for paleoprecipitation (CIA-K, CALMAG and PPM model) and paleotemperature (Salinization and PPM model) yielded very low estimates (Table 1) that seem unreasonable given that the region is within the equator where MAT is above 25°C and MAP range from 1000 to 2000 mm/yr. The best estimates for MAP is likely at the range of 1000-1200 mm/yr. for humid conditions, which falls within the values estimated from paleo-Vertisols which showed no evidence of diagenetic calcite.

Results from the PPM model are reasonable for the Koru 21 site with values ranging from 1090-1968 mm (Table 1) for a humid climatic zone.

The low estimates of MAP are attributed to the poor weathering of volcanic minerals, poor leaching of base cations and rapid sedimentation rate that outpaced pedogenic processes. The presence of slickensides, illuviated clay and pedogenic carbonate suggests wet and dry conditions or seasonal precipitation.

MAT estimates from NaK and PPM model are very low as well (Table 1) given that the Tinderet locality is within an equatorial setting. As Lukens et al. (2017) reported the MAT for Karungu NG15 sites, we suggests that Tinderet sites MAT was probably warmer as well and similar to fossil leaves estimates from Rusinga Island of 23-35°C (Michel et al., 2014). Lukens et al. (2017) and Stinchcomb et al. (2016) pointed out that MAT estimates from elemental proxies are often below reasonable estimates primarily because MAT is less important in controlling soil weathering as compared to other variables such as precipitation.

Paleoenvironment Reconstruction

While accounting for the $\delta^{13}C$ of atmospheric CO_2 during the early Miocene (Passey et al., 2002; Tipple et al., 2010), the $\delta^{13}C$ values of soil organic matter from the three sites indicate a mixture of the two end members, that is, C_3 and C_{3ws} (Fig. 12). This mixture could be attributed to contribution from C_4 biomass. Comparing the $\delta^{13}C$ values to the compilation of $\delta^{13}C$ of soil organic matter from different ecosystems (Cerling et al., 2010), the isotopic signature of Koru 16, Koru 21 and Kapurtay New is similar to modern dry deciduous forest environments.

Presence of tree stump casts, fossilized tree branches, roots and fossil leaves in Koru 16 forest paleosol interval, enabled us to utilize a high resolution method used by Michel et al. (2014) to reconstruct the habitat preference for the primates dating back to early Miocene. Reconstructing the forest structure using the basal area (≥13.7 m^2/ha) and density of tree stump casts (≥136 trees/ha) suggests that this interval represents a patch for a less dense tropical forest with young and mature trees. These values are similar to other present-day forests with primates such as the Yasuni forest in Ecuador and Huai Kha Khaeng forest in Thailand (Table 1). However, the Koru 16 forest does not include trees with ≥60 cm dbh which were found in Rusinga Island (Michel et al., 2014) and are common in modern day older tropical forests. This suggests that Koru 16 probably sampled a younger forest with breaks in the canopy.

Micromorphology of Kapurtay New and Koru 16 revealed a lot of charcoal (Fig. 10C) which suggests occasional occurrence of wildfires during the dry seasons. Similar occurrence is also reported in Karungu NG15 paleosols (Lukens et al., 2017) which is linked to seasonal aridity. The charcoal grains are small enough to be eolian or fluvial deposits but given the angularity of the charcoal grains and that the other environmental indicators suggests a forested environment, it is more likely that the charcoal grains originated locally.

Implications for Hominoid Evolution

As noted by Cote (2008), there are differences in the distribution of catarrhine and non-catarrhine mammal species among the Tinderet sites with Kapurtay accounting for more primate diversity as compared to other sites such as Koru, Songhor and Napak localities. From the paleoecological methods used by Evans et al. (1981) and Cote

(2008), there is little to no variation in the environment even while accounting for the presence of species indicators. In particular, Cote (2008), using multivariate analysis, found no consistent patterns in species representation across the sites (i.e. species that are more frequent appearing or not appearing together).

My results revealed similar interpretations and demonstrate that there is little to no environmental variation between Koru and Kapurtay sites that document a landscape associated with a seasonally dry forest. This indicates that environmental differences are unlikely to explain the differences in species distribution between the sites.

CHAPTER FIVE

Conclusion

Detailed paleopedological, stratigraphic and sedimentological analyses of Koru and Kapurtay sites demonstrate a history of a disturbed landscape that experienced short periods of soil development followed by abrupt ash deposition from the Tinderet volcano eruptions. Paleoenvironment reconstructed using stable isotopes and tree stump casts, which is similar for all the sites, is consistent with a seasonally dry tropical seasonal forest with breaks in the canopy. The tropical seasonal forest existed in a climate with a MAT >14°C and MAP >1000 mm/yr. At all of the sites, sedimentation rates were faster than pedogenesis and this resulted to the abundance of unweathered volcanic minerals that contributed significantly to the underestimation of MAT and MAP.

The presence of Fe and Mn depleted zones and reprecipitated calcite in pore spaces for Koru paleosols could be linked to water logged conditions from high precipitation or ground water movement. Occurrence of charcoal in Kapurtay and Koru 16 paleosols are likely linked to wildfires that facilitated the maintenance of the landscape, a phenomenon common in seasonally dry forests with canopy breaks.

I find no link between the variation in the distribution of catarrhine and non-catarrhine mammals to the environment since this was a constant factor across the localities. To account for the variation in faunal assemblage, we present a testable hypothesis that the Koru and Kapurtay sites are of different ages and by using

paleomagnetic analysis we can test the polarity of the sites to determine how similar or different the sites are in age.

APPENDIX

Table 3. Elemental geochemistry for Koru 16, Koru 21 and Kapurtay New.

Profile	Horizon	Al_2O_3	CaO	Fe_2O_3	K_2O	MgO	MnO	Na_2O	P_2O_5	SiO_2	TiO_2	ZrO_2
Koru 16 site												
K16/01	Bt2	12.85	2.9	11.65	2.13	2.85	0.22	0.74	0.73	48.3	2.12	0.04
K16/02	Btss2	6.73	29.2	6.2	1.11	1.67	0.2	0.4	1.3	24	1.12	0.03
K16/03	Bss2	12.3	4.56	12.2	1.98	2.96	0.11	0.78	0.94	47.5	2.05	0.04
K16/04	Bw4	12.55	2.95	10.9	3.07	2.68	0.07	1.41	0.83	53.7	1.69	0.05
K16/05	Bw3	9.59	12.65	11.35	2.73	2.65	0.32	0.78	1.01	39.1	1.98	0.04
K16/06	Bt1	11.45	6.89	9.17	2.62	2.36	0.09	1.19	0.81	48.4	1.2	0.04
K16/07	Bt1	10.8	10.6	8.46	2.21	2.41	0.18	1.19	1.87	44.7	1.43	0.04
K16/08	Btss1	12.8	3.88	10.15	2.53	2.82	0.08	1.04	0.98	52.6	1.55	0.05
K16/09	Bw2	11.4	8.72	8.04	2.69	2.34	0.08	1.21	0.53	48.3	1.32	0.04
K16/10	Bw1	12.5	3.52	9.25	3.25	2.81	0.09	1.56	0.81	54	1.35	0.04
Koru 21 site												
K20/01	Bw3	13.3	6.16	10.45	2.23	1.85	0.77	1.07	1.16	47.2	1.4	0.04
K20/02	Bw3	12.3	6.48	12.3	1.99	2.07	0.35	0.55	1.86	45.3	1.22	0.04
K20/03	Bw2	10.7	13.9	9.36	2.27	2.26	0.29	1.1	1.23	37.4	1.13	0.03
K20/04	Bw2	11.75	10.55	9.75	2.29	2.26	0.39	1.3	1.17	41.4	1.37	0.03
K20/05	Bw1	7.48	23.9	9.91	1.25	1.63	0.37	0.62	1.5	26.4	0.98	0.02
Kapurtay New site												
KP/01	Bw1	12.8	5.02	12.8	2.96	3.8	0.17	1.53	1.65	47.2	1.53	0.03
KP/02	Bw3	10.4	8.14	10.6	1.62	6.21	0.17	1.16	0.51	43.1	1.51	0.02

Table 4. Stable carbon isotope and organic carbon analyses.

Sample Number	Depth (m)	Horizon	$\delta^{13}C$	Organic C wt. %
Koru 21 site				
K21 01	-3.04	Bw3	-20.61	0.03
K21 02	-3.19	Bw3	-25.64	0.06
K21 04	-3.81	Bw2	-22.71	0.13
K21 05	-3.63	Bw1	-24.62	0.04
K21 06	-4.51	Bw1	-24.86	0.05
Koru 16 site				
K16 01	-0.07	Bt2	-21.68	0.13
K16 02	-0.27	Btss2	-24.51	0.04
K16 03	-0.37	Bss2	-23.93	0.03
K16 04	-4.03	Bw3	-23.76	0.04
K16 07	-5.23	Bw2	-22.64	0.03
K16 08	-5.56	Btss1	-23.43	0.03
K16 09	-5.76	Bt1	-24.76	0.06
Kapurtay New site				
KP 01	-11.14	Bw1	-24.64	0.11
KP 03	-6.4	Bw3	-22.64	0.15

Descriptions of Paleosol Profiles

Koru 16A Paleosol

Koru 16 comprises multiple paleosols interbedded by ash deposits. The basal unit is a paleo-vertisol that is 37 cm thick, and a sharp, undulating, erosive contact with the overlying coarse-grained weathered ash deposit (unit 2). The lower contact is covered.

Bss2 horizon: 0 to 7 cm, clayey siltstone, noncalcareous; matrix is 2.5YR 4/6 (red); MnO-coated slickenside surfaces, Fe oxide nodules; fine to medium root traces; medium to fine angular wedge shaped peds.

Btss2 horizon: **7**-27 cm, variegated clayey siltstone, noncalcareous; matrix is 80% 2.5YR 4/6 (red), and 20% 5Y 4/1 (dark gray) fine root mottle; MnO-coated slickenside surfaces, Fe oxide nodules; illuviated clay; fine root traces; angular wedge shaped peds.

Bt2 horizon: 27-37 cm, variegated clayey siltstone, noncalcareous; mottled matrix is 90% 2.5YR 4/6 (red) and 10% 5Y 6/1 (gray) fine root mottle; fine to medium root traces; moderate fine wedge peds; illuviated clay.

Bw4 horizon: 169-206 cm, fine grained sandstone, calcareous, matrix is 7.5YR 3/4, fine root mottles; fine to medium angular blocky peds, clear smooth contact with the underlying and overlying units (5 & 7).

Bw3 horizon: 206-473 cm, coarse grained sandstone, highly calcareous, horizontal lamination characterize the matrix with color ranging from 10YR 7/8 (yellow), Gley 1 6/10Y and 6/5GY; coarse root mottles; medium platy peds; clear smooth contact with the

underlying and overlying units; calcified tree stump casts, tree branches, roots and fossil leaves; accretionary lapilli weathered into clay in the lower section of the unit; lamination increase in thickness upwards.

Bw2 horizon: 473-493 cm, fine to medium grained sandstone, calcareous, matrix is 7.5YR 3/4, fine root mottles; fine to medium angular blocky peds, clear smooth contact with the underlying and diffused contact with the overlying horizon.

Btss1 horizon: 493-513 cm, variegated clayey sandstone, calcareous; matrix is 90% 10R 4/6 (red), and 10% 5Y 4/1 (dark gray) coarse drab haloed root traces; slickenside surfaces; illuviated clay; Fe oxide nodules; fine root traces; coarse angular wedge shaped peds.

Bt1 horizon: 513-546 cm, clayey sandstone, calcareous; matrix is 5YR 4/4 (reddish brown) with medium angular blocky ped structure; fine root traces and illuviated clay along root traces.

Bw1 horizon: 577-605 cm, silty sandstone, calcareous; matrix is 80% 2.5YR 6/6 (red) with 20% 5GY 8/1 (light greenish gray) fine root mottles; moderate fine angular blocky peds, unweathered volcanic minerals such as mica; clear smooth contact.

Note: Site B not described due to modern imprints. However, the two profiles were correlated using the lithology of unit 7 in site A. See figure 4.

Koru 21 Paleosols

Koru 21 lithology comprises compound paleosols bounded by lithified carbonatite ash deposits. The boundary contact between the paleosol and ash deposits is sharp and undulating.

Bw3 horizon: 289-319 cm, sandstone, calcareous, matrix is 5YR 4/4 (reddish brown) with fine root mottles; abundant in unweathered volcanic minerals such as mica; angular wedge peds; sharp undulating contact with the underlying unit 1.

BC2 horizon: 319-345 cm, sandstone, highly calcareous, matrix is 80% 5YR 6/3 (light reddish brown) and 20% 2.5YR 5/4 (reddish brown) with some fine root mottles; abundant in unweathered volcanic minerals such as mica; angular blocky ped structure.

Bw2 horizon: 345-380 cm, medium sandstone, highly calcareous, matrix is 80% 7.5YR ¾ with fine root mottles; fine to medium wedge ped structure; unweathered volcanic minerals such as mica.

BC1 horizon: 380-396 cm, coarse sandstone, highly calcareous, matrix is 80% 5YR 6/3 (light reddish brown) and 20% 2.5YR 5/4 (reddish brown) with some fine root mottles; abundant in unweathered volcanic minerals such as mica; angular blocky ped structure.

Bw1 horizon: 396-453 cm, medium sandstone, calcareous, matrix is 5YR 4/4 (reddish brown) with fine root mottles; abundant in unweathered volcanic minerals such as mica; medium wedge peds; sharp undulating upper contact with the overlying ash deposit.

Kapurtay New Paleosols

Kapurtay New site comprises weakly developed paleosols interbedded by ash deposits. These paleosols are much thinner and more abundant in unweathered volcanic minerals as compared to Koru paleosols.

Bw3 horizon: 400-640 cm, medium sandstone, calcareous, matrix is 90% 2.5YR 5/4 (reddish brown) with fine to medium root mottles; Fe oxide nodules, Mn oxide on ped faces, abundant in unweathered volcanic minerals such as mica; fine wedge peds; lower contact is covered.

Bw2 horizon: 104-114 cm, medium sandstone, highly calcareous, matrix is 90% 2.5YR 5/4 (reddish brown) with 10% 5Y 4/1 (dark gray) fine root traces; Fe oxide nodules, medium wedge peds with Mn oxide on surfaces; unweathered volcanic minerals such as mica; sharp and wavy contact between the bounding units (5 & 7).

Bw1 horizon: 119-124 cm, medium sandstone, highly calcareous, matrix is 2.5YR 5/4 (reddish brown) with very fine root mottle; unweathered volcanic minerals, Fe oxide nodules and Mn oxide on ped faces; fine wedge ped structure, sharp and wavy lower and upper contacts.

BIBLIOGRAPHY

Andrews, P., and Kelley, J., 2007, Middle Miocene Dispersals of Apes: Folia Primatologica, v. 78, p. 328–343, doi: 10.1159/000105148.

Brewer, R., 1964, Fabric and mineral analysis of soils: New York : John Wiley, https://trove.nla.gov.au/work/10889583 (accessed February 2018).

Bullock, P., etc, and Science, I.S. of S., 1985, Handbook for Soil Thin Section Description: Albrighton, Waine Research Publications, 152 p.

Casanovas-Vilar, I., Alba, D.M., Garces, M., Robles, J.M., and Moya-Sola, S., 2011, Updated chronology for the Miocene hominoid radiation in Western Eurasia: Proceedings of the National Academy of Sciences, v. 108, p. 5554–5559, doi: 10.1073/pnas.1018562108.

Cerling, T.E., Harris, J.M., MacFadden, B.J., Leakey, M.G., Quade, J., Eisenmann, V., and Ehleringer, J.R., 1997, Global vegetation change through the Miocene/Pliocene boundary: Nature, v. 389, p. 153–158, doi: 10.1038/38229.

Cerling, T.E., Levin, N.E., Quade, J., Wynn, J.G., Fox, D.L., Kingston, J.D., Klein, R.G., and Brown, F.H., 2010, Comment on the Paleoenvironment of Ardipithecus ramidus: Science, v. 328, p. 1105–1105, doi: 10.1126/science.1185274.

Cote, S.M., 2004, Origins of the African hominoids: an assessment of the palaeobiogeographical evidence: Comptes Rendus Palevol, v. 3, p. 323–340, doi: 10.1016/j.crpv.2004.03.006.

Cote, S.M., 2008, Sampling and ecology in three Early Miocene catarrhine assemblages from East Africa: Harvard University.

Deans, T., and Roberts, B., 1984, Carbonatite tuffs and lava clasts of the Tinderet foothills, western Kenya: a study of calcified natrocarbonatites: Journal of the Geological Society, v. 141, p. 563–580.

Ehleringer, J.R., 1978, Implications of quantum yield differences on the distributions of C3 and C4 grasses: Oecologia, v. 31, p. 255–267, doi: 10.1007/BF00346246.

Ehleringer, J.R., and Cooper, T.A., 1988, Correlations between carbon isotope ratio and microhabitat in desert plants: Oecologia, v. 76, p. 562–566, doi: 10.1007/BF00397870.

Ehleringer, J.R., and Monson, R.K., 1993, Evolutionary and Ecological Aspects of Photosynthetic Pathway Variation: Annual Review of Ecology and Systematics, v. 24, p. 411–439, doi: 10.1146/annurev.es.24.110193.002211.

Elton, S., 2007, Environmental Correlates of the Cercopithecoid Radiations: Folia Primatologica, v. 78, p. 344–364, doi: 10.1159/000105149.

Evans, E.M.N., Van Couvering, J.A.H., and Andrews, P., 1981, Palaeoecology of Miocene sites in Western Kenya: Journal of Human Evolution, v. 10, p. 99–116, doi: 10.1016/S0047-2484(81)80027-9.

Harrison, T., 1982, Small-bodied apes from the Miocene of East Africa [PhD Thesis]: University of London Ph. D. thesis.

Hopwood, A.T., 1933, Miocene Primates from Kenya.: Zoological Journal of the Linnean Society, v. 38, p. 437–464.

Jablonski, N.G., 2005, Primate homeland: forests and the evolution of primates during the Tertiary and Quaternary in Asia: Anthropological Science, v. 113, p. 117–122, doi: 10.1537/ase.04S016.

Kohn, M.J., 2010, Carbon isotope compositions of terrestrial C3 plants as indicators of (paleo)ecology and (paleo)climate: Proceedings of the National Academy of Sciences, v. 107, p. 19691–19695, doi: 10.1073/pnas.1004933107.

Leakey, M., Grossman, A., Gutiérrez, M., and Fleagle, J.G., 2011, Faunal Change in the Turkana Basin during the Late Oligocene and Miocene: Evolutionary Anthropology: Issues, News, and Reviews, v. 20, p. 238–253, doi: 10.1002/evan.20338.

Lukens, W.E., Lehmann, T., Peppe, D.J., Fox, D.L., Driese, S.G., and McNulty, K.P., 2017, The Early Miocene Critical Zone at Karungu, Western Kenya: An Equatorial, Open Habitat with Few Primate Remains: Frontiers in Earth Science, v. 5, doi: 10.3389/feart.2017.00087.

Martin, L., 1981, New specimens of Proconsul from Koru, Kenya: Journal of Human Evolution, v. 10, p. 139–150, doi: 10.1016/S0047-2484(81)80011-5.

Michel, L.A., Peppe, D.J., Lutz, J.A., Driese, S.G., Dunsworth, H.M., Harcourt-Smith, W.E.H., Horner, W.H., Lehmann, T., Nightingale, S., and McNulty, K.P., 2014, Remnants of an ancient forest provide ecological context for Early Miocene fossil apes: Nature Communications, v. 5, doi: 10.1038/ncomms4236.

Moore, D.M., and Reynolds, R.C., 1997, X-Ray Diffraction and the Identification and Analysis of Clay Minerals: Oxford ; New York, Oxford University Press.

Nordt, L.C., and Driese, S.D., 2010, New weathering index improves paleorainfall estimates from Vertisols: , p. 4.

Odom, I.E., 1984, Smectite clay Minerals: Properties and Uses: Philosophical Transactions of the Royal Society A: Mathematical, Physical and Engineering Sciences, v. 311, p. 391–409, doi: 10.1098/rsta.1984.0036.

O'Leary, M.H., 1981, Carbon isotope fractionation in plants: Phytochemistry, v. 20, p. 553–567, doi: 10.1016/0031-9422(81)85134-5.

O'Leary, M.H., 1988, Carbon Isotopes in PhotosynthesisFractionation techniques may reveal new aspects of carbon dynamics in plants: BioScience, v. 38, p. 328–336, doi: 10.2307/1310735.

Passey, B.H., Cerling, T.E., Perkins, M.E., Voorhies, M.R., Harris, J.M., and Tucker, S.T., 2002, Environmental Change in the Great Plains: An Isotopic Record from Fossil Horses: The Journal of Geology, v. 110, p. 123–140, doi: 10.1086/338280.

Pickford, M., and Andrews, P., 1981, The Tinderet Miocence sequence in Kenya: Journal of Human Evolution, v. 10, p. 11–33.

Poppe, L.J., Paskevich, V.F., Hathaway, J.C., and Blackwood, D.S., 2001, A laboratory manual for X-ray powder diffraction: US Geological Survey Open-File Report, v. 1, p. 1–88.

Schoeneberger, P.J., 2012, Field book for describing and sampling soils: Government Printing Office.

Sheldon, N.D., Retallack, G.J., and Tanaka, S., 2002, Geochemical Climofunctions from North American Soils and Application to Paleosols across the Eocene-Oligocene Boundary in Oregon: The Journal of Geology, v. 110, p. 687–696, doi: 10.1086/342865.

Soil Survey Staff, 2010, Keys to Soil Taxonomy: USDA.

Stewart, C.-B., and Disotell, T.R., 1998, Primate evolution–in and out of Africa: Current Biology, v. 8, p. R582–R588.

Stinchcomb, G.E., Nordt, L.C., Driese, S.G., Lukens, W.E., Williamson, F.C., and Tubbs, J.D., 2016, A data-driven spline model designed to predict paleoclimate using paleosol geochemistry: American Journal of Science, v. 316, p. 746–777, doi: 10.2475/08.2016.02.

Tipple, B.J., Meyers, S.R., and Pagani, M., 2010, Carbon isotope ratio of Cenozoic CO2: A comparative evaluation of available geochemical proxies: Paleoceanography, v. 25, doi: 10.1029/2009PA001851.

Zaitsev, A.N., Wenzel, T., Vennemann, T., and Markl, G., 2013, Tinderet volcano, Kenya: an altered natrocarbonatite locality? Mineralogical Magazine, v. 77, p. 213–226, doi: 10.1180/minmag.2013.077.3.01.